AGU PUBLICATIONS

JGR

Journal of Geophysical Research: Space Physics

RESEARCH ARTICLE

10.1002/2013JA019168

**Key Points:**

- The cold ions ($H^+$, $He^+$, and $O^+$) are picked up by the reconnected magnetic field
- The cold ions are accelerated perpendicular to the magnetic field
- Asymmetric reconnection geometry is caused by the stronger asymmetry in density

**Correspondence to:**
H. Zhang,
hzhang@gi.alaska.edu

**Citation:**
Lee, S. H., H. Zhang, Q.-G. Zong, A. Otto, D. G. Sibeck, Y. Wang, K.-H. Glassmeier, P. W. Daly, and H. Rème (2014), Plasma and energetic particle behaviors during asymmetric magnetic reconnection at the magnetopause, *J. Geophys. Res. Space Physics*, *119*, 1658–1672, doi:10.1002/2013JA019168.

Received 28 JUN 2013
Accepted 11 FEB 2014
Accepted article online 14 FEB 2014
Published online 6 MAR 2014

# Plasma and energetic particle behaviors during asymmetric magnetic reconnection at the magnetopause

**S. H. Lee[1], H. Zhang[1], Q.-G. Zong[2], A. Otto[1], D. G. Sibeck[3], Y. Wang[2], K.-H. Glassmeier[4], P. W. Daly[5], and H. Rème[6,7]**

[1]Geophysical Institute, University of Alaska, Fairbanks, Alaska, USA, [2]Institute of Space Physics and Applied Technology, School of Earth and Space Sciences, Peking University, Beijing, China, [3]NASA Goddard Space Flight Center, Greenbelt, Maryland, USA, [4]Institute for Geophysics and Extraterrestrial Physics, Braunschweig, Germany, [5]Max Planck Institute for Solar System Research, Katlenburg-Lindau, Germany, [6]University of Toulouse, UPS-OMP, IRAP, Toulouse, France, [7]CNRS, IRAP, Toulouse, France

**Abstract** The factors controlling asymmetric reconnection and the role of the cold plasma population in the reconnection process are two outstanding questions. We present a case study of multipoint Cluster observations demonstrating that the separatrix and flow boundary angles are greater on the magnetosheath than on the magnetospheric side of the magnetopause, probably due to the stronger density than magnetic field asymmetry at this boundary. The motion of cold plasmaspheric ions entering the reconnection region differs from that of warmer magnetosheath and magnetospheric ions. In contrast to the warmer ions, which are probably accelerated by reconnection in the diffusion region near the subsolar magnetopause, the colder ions are simply entrained by $\mathbf{E}\times\mathbf{B}$ drifts at high latitudes on the recently reconnected magnetic field lines. This indicates that plasmaspheric ions can sometimes play only a very limited role in asymmetric reconnection, in contrast to previous simulation studies. Three cold ion populations (probably $H^+$, $He^+$, and $O^+$) appear in the energy spectrum, consistent with ion acceleration to a common velocity.

## 1. Introduction

Magnetic reconnection is a universal process that converts stored magnetic energy into particle kinetic energy and produces changes in the magnetic topology. It is primarily invoked to transfer momentum and energy from the solar wind to the magnetosphere at Earth's magnetopause [*Dungey*, 1961; *Sonnerup et al.*, 1987]. If the magnitude of the magnetic field and the plasma density on both sides of the current sheet are similar, the magnetic reconnection is defined as symmetric reconnection [*Mozer et al.*, 2008; *Mozer and Pritchett*, 2009]. Symmetric reconnection is usually characterized by a quadrupolar out-of-plane magnetic field component and a bipolar normal electric field [*Øieroset et al.*, 2001; *Mozer et al.*, 2002].

At the dayside magnetopause, the solar wind plasma density is generally much higher than that inside the magnetosphere and the magnitude of the interplanetary magnetic field (IMF) is much weaker than that of the terrestrial field. Thus, dayside reconnection occurring at the subsolar region is generally characterized by asymmetric plasma and magnetic field conditions. For reconnection occurring at the dayside subsolar region, the magnitude of the reconnecting magnetic field and plasma density may vary more than an order of the magnitude across the dayside magnetopause current layer, leading to the magnetic field and the plasma flow geometries being very different from those associated with symmetric reconnection. The scaling analyses for the reconnection rate, outflow speed, the density of the outflow, and the structure of the dissipation region during asymmetric magnetic reconnection have been investigated with different simulation models [*Pritchett and Mozer*, 2009; *Birn et al.*, 2008; *Borovsky and Hesse*, 2007] and theories [*Cassak and Shay*, 2007, 2008, 2009].

Magnetic topological changes are to be expected once the IMF on the magnetosheath side becomes magnetically connected to the magnetic field on the magnetospheric side, and the accelerated plasma jets away from the reconnection region. The reconnection separatrix is defined as the field line connected to the X line, and it is located close to the electron edge which is a boundary of both transmitted and mirrored electrons, whereas the flow boundary is a boundary between inflow and the outflow jet, and it approximately coincides with the ion edge. Electrons move much faster than ions while both electrons and ions convect

with the magnetic field by the $\mathbf{E} \times \mathbf{B}$ drift, so the electron boundaries are more closely field aligned than the ion boundaries. Two boundaries, the separatrix and the flow boundary, have been identified by taking into account kinetic effects during magnetic reconnection [*Øieroset et al.*, 2001; *Retinò et al.*, 2006; *Lindstedt et al.*, 2009; *Gosling et al.*, 1990b].

The topology of magnetic reconnection can be deduced from either the magnetic separatrix angles or the plasma flow boundary angles. Identifying the boundaries (the separatrix and the flow boundary) is important in order to obtain the angles of the separatrix and the flow boundary on both sides of the current sheet, and the magnetic reconnection rate can be estimated by measuring the ratio of the inflow velocity to the asymptotic Alfvén speed which is related to the separatrix angle [*Xiao et al.*, 2007].

Until now, few studies on the dayside reconnection have considered the plasma and energetic particle behaviors during asymmetric magnetic reconnection at the magnetopause. Energetic particles have been observed during magnetic reconnection events in various astrophysical environments, such as solar flares, the magnetotail, and the magnetopause [*Lin et al.*, 2003; *Øieroset et al.*, 2002; *Zhang et al.*, 2008]. Some studies have explored the acceleration mechanisms for the presence of the energetic ions in the reconnection region [*Speiser et al.*, 1981; *Cowley*, 1982; *Zong and Wilken*, 1998, 1999; *Zong et al.*, 2001]. However, different aspects of energetic particle behavior during symmetric and asymmetric reconnection are still little explored. On the other hand, cold and dense plasmaspheric plasma at the dayside magnetopause has been investigated by several studies [*Su et al.*, 2000; *Borovsky and Steinberg*, 2006; *Borovsky and Denton*, 2006; *Cowley*, 1982; *Gosling et al.*, 1990a; *André et al.*, 2010]. We find some important characteristics of the accelerated cold dense ions and their effect on the reconnection dynamics which is related to the previous observational and simulation studies [*Gosling et al.*, 1990a; *Borovsky and Denton*, 2006; *Borovsky et al.*, 2008].

Here we present Cluster observations of the magnetic reconnection event at the dayside magnetopause to illustrate the asymmetric reconnection topology with identification of the separatrices and flow boundaries on the magnetosheath and magnetospheric sides and study the cold ion and energetic particle behaviors during asymmetric magnetic reconnection at the magnetopause. The outline of this paper is as follows. In section 2, we describe the geometry of the magnetic reconnection and cold and energetic ion behaviors during reconnection. In section 3, we discuss the asymmetric reconnection geometry and effect of cold ions on the reconnection dynamics. Section 4 contains the summary and conclusions of this paper.

## 2. Cluster Observations and Interpretation

### 2.1. Data Sets and Method

Cluster [*Escoubet et al.*, 1997] is a mission that consists of four identical satellites flying in a tetrahedral-like formation. In this paper we use data from several instruments on board Cluster: the spin-resolution (4 s) ion data from the Hot Ion Analyzer (HIA) measurements from the Cluster Ion Spectrometry (CIS) experiment [*Rème et al.*, 2001]; the magnetic field data from the fluxgate magnetometer (FGM) at a resolution of 0.004 s [*Balogh et al.*, 1997]; electric field spectrogram from Spatiotemporal Analysis of Field Fluctuations (STAFF) [*Cornilleau-Wehrlin et al.*, 2003] in the frequency range of 8 Hz–4 kHz with a time resolution of 1 s; electron energy spectrogram from the plasma electron and current experiment (PEACE), which is measured in a sequence of spins; and 3-D energetic electron and ion fluxes from the Research with Adaptive Particle Imaging Detectors (RAPID) [*Wilken et al.*, 2001].

Figure 1 illustrates the Cluster orbit from 18:00 to 20:00 UT on 5 March 2007. Cluster 3 (C3, green star) was located primarily inside the magnetosphere and crossed the magnetopause at ($X$, $Y$, and $Z$) = (8.1, 1.3, and 4.5) $R_E$ in the GSM reference frame. While traveling outbound in the northern hemisphere, Cluster crossed the magnetopause several times and exited to the magnetosheath. The inner and outer red lines indicate the locations of the magnetopause and bow shock determined by the Fairfield model [*Fairfield*, 1971].

The separatrix and the flow boundary have been identified by using flow, particles, and wave data [*Retinò et al.*, 2006; *Gosling et al.*, 1990b; *Vaivads et al.*, 2010; *Retinò et al.*, 2006; *Matsumoto et al.*, 2003; *Cattell et al.*, 2005; *Deng and Matsumoto*, 2001]. Both wave and particles data have been used to identify the separatrix. The first transmitted electrons may induce plasma instabilities which generate wave emissions. Hence, the separatrix can be found as a boundary in wave activity features where the waves become more intense and broadband [*Retinò et al.*, 2006]. Similarly, *Matsumoto et al.* [2003] have observed enhanced broadband electrostatic emissions, such as Electrostatic Solitary Waves and Amplitude Modulated Electrostatic Waves with high-speed spikes of the plasma velocities, related to the reconnection along the dayside magnetopause.

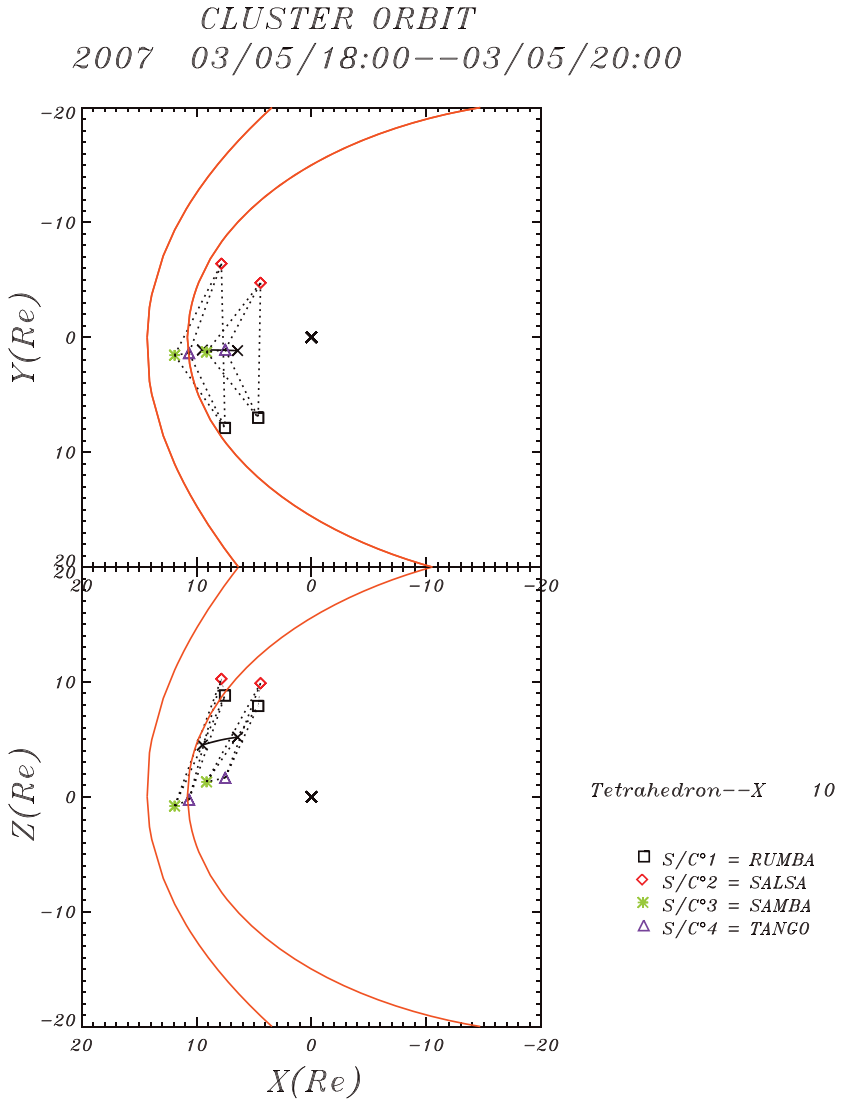


**Figure 1.** Cluster orbit in the *X-Z* and *X-Y* GSM plane from 18:00 UT to 20:00 UT on 5 March 2007. The tetrahedron configuration is enlarged by 10 times. The locations of the magnetopause and the bow shock, which are determined by the Fairfield model, are marked by the red lines.

Large-amplitude solitary waves have been observed by the Cluster spacecraft at multiple locations along the separatrices associated with magnetotail reconnection [*Cattell et al.*, 2005]. *Retinò et al.* [2006] have also identified the magnetic separatrix by taking a sharp boundary in electric field waveforms using the Wideband Plasma Wave Investigation. *Lindstedt et al.* [2009] and *Vaivads et al.* [2010] defined the electron edge or separatrix on the magnetospheric side where the first magnetosheath electrons or parallel electrons with a typical energy of hundreds of eV are observed. The flow boundary has been defined by the density gradient, first observed magnetosheath ions on the magnetospheric side, a sharp change in the ion distribution, the plasma flow $V_L$ component increases [*Lindstedt et al.*, 2009; *Gosling et al.*, 1990b], and the thermal speed of plasmas [*Vaivads et al.*, 2010] by using the flow and particles data.

### 2.2. Overview

Figure 2 shows magnetic field data from Wind and plasma and magnetic field data from Cluster 3 for an outbound crossing of the magnetopause on 5 March 2007. The solar wind speed was around 400 km/s as detected by the Wind satellite at ($X$, $Y$, and $Z$)$_{GSM}$ = (200, −57.5, and −43) $R_E$ during the magnetic reconnection at the dayside magnetopause. Therefore, the solar wind parameters are shifted by about 64 min to match the Cluster magnetic field measurements. The IMF ($B_x$, $B_y$, and $B_z$) was (−4, 1, and −4) nT (Figure 2a),

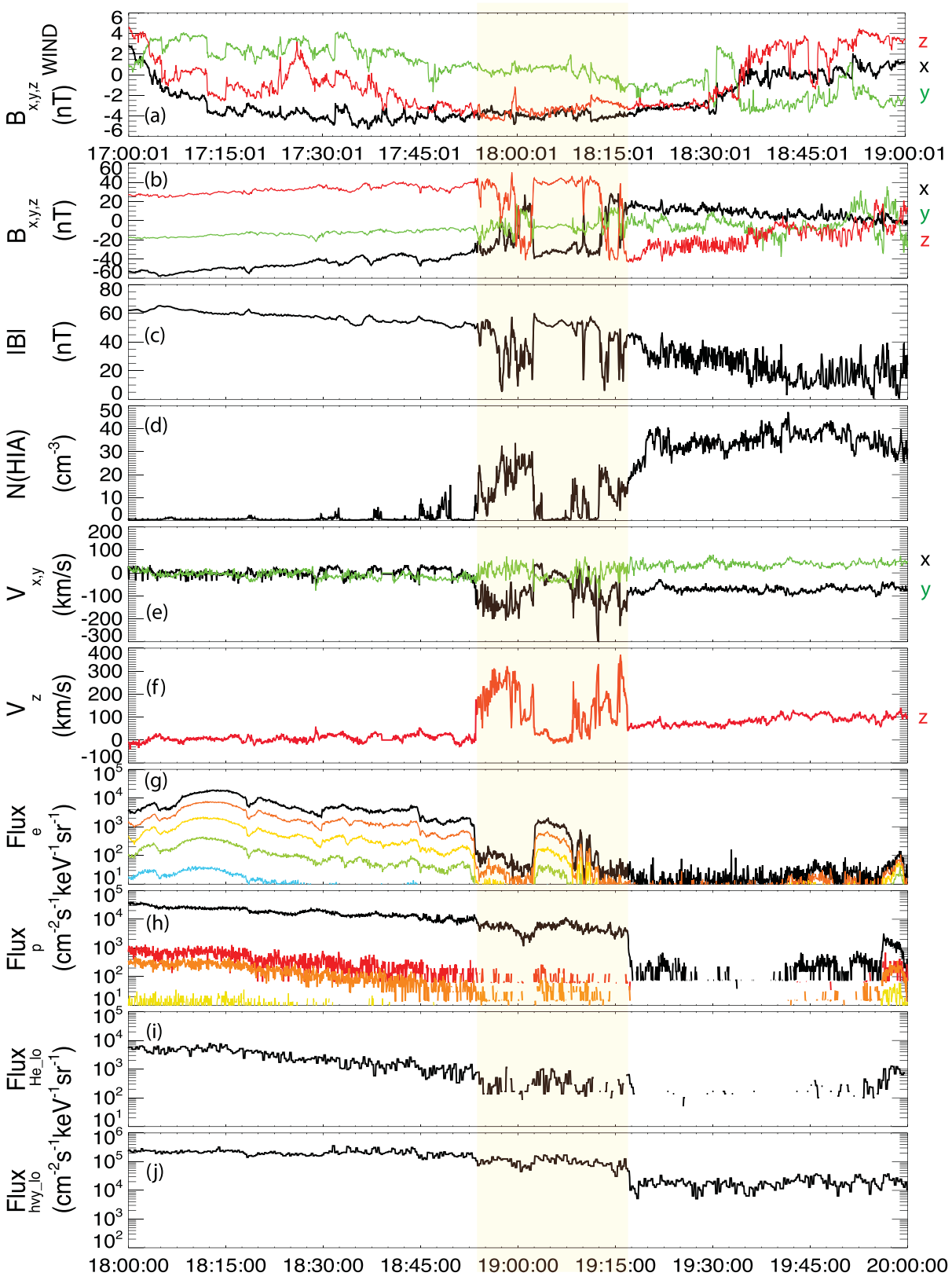


**Figure 2.** Field and plasma data from multiple magnetopause crossings collected by C3 from 18:00 UT to 20:00 UT on 5 March 2007. (a) Time-shifted (by 1 h) interplanetary magnetic field (IMF) in the GSM coordinate from Wind satellite; (b) magnetic field in the GSM coordinates (*x* component, black; *y*, green; and *z*, red); (c) total magnetic field; (d) ion density; (e) plasma flow, $V_x$ and $V_y$ components; (f) $V_z$ component in the GSM coordinates; and (g–j) differential particle flux of electrons, protons, helium (> 30 keV), and heavy ions (> 84 keV).

the geomagnetic activity index (*Dst*) was −9 nT, the dynamic pressure was less than 3 nPa, and the *Kp* index was 4, indicating a moderately quiet magnetosphere (not shown). The spacecraft crossed the magnetopause several times, which can be identified by the sign change in $B_z$ from positive (magnetosphere) to negative (magnetosheath) or the opposite (Figure 2b). The magnetic field strength (Figure 2c), the plasma density, and three components of the plasma velocity from the CIS instrument are shown in Figures 2d–2f. The ratio of the magnetic field strength on the magnetospheric side to that on the magnetosheath side is approximately 1.2, and the density ratio is about 1/13. The high-speed flow peaked at 350 km/s was observed from 18:50:00 UT to 19:20:00 UT (Figure 2f). It satisfies the Walén relation, indicating the spacecraft being in the reconnection exhaust region [*Paschmann et al.*, 1979; *Sonnerup et al.*, 1981]. Flow velocity in the de Hoffmann-Teller (dHT) frame is highly correlated (0.93) with the local Alfvén velocity from 19:00:30 UT to 19:01:00 UT (not shown). The differential fluxes of energetic electrons, protons, helium (>30 keV), and heavy ions (> 84 keV) from the RAPID instrument are shown in Figures 2g–2j.

### 2.3. Geometry of the Magnetic Reconnection

Figure 3 shows C3 data from 19:00:00 UT to 19:20:00 UT. The bars at the top mark three different regions: the magnetosphere (Msp), the magnetosheath (Msh), and the boundary layer (BL). The ion energy spectrogram from CIS-HIA high-sensitivity data shows a mixture of the magnetosheath (∼1 keV) and magnetospheric (∼10 keV) ions in the boundary layer, pure magnetospheric ion (∼10 keV) in the magnetosphere, and pure magnetosheath ion (∼1 keV) in the magnetosheath (Figure 3a). The electron differential flux parallel and antiparallel to the magnetic field (4 s time resolution) from the PEACE instrument can also be used to distinguish different regions (Figures 3b–3d). In the boundary layer there are both magnetospheric (∼10 keV) and magnetosheath (∼100 eV) electrons and ions. High-speed flow, $V_L \sim 350$ km/s, was observed in the boundary layer (Figure 3e). The *L* component of the magnetic fields ($B_L$) changed its sign several times, indicating that C3 crossed the current sheet several times. The boundary normal coordinates ($L_{GSE}$ = (−0.526, 0.298, and 0.797), $M_{GSE}$ = (−0.003, −0.937, and 0.348), and $N_{GSE}$ = (0.850, 0.181, and 0.494)), which were determined by the minimum variance analysis (MVA) of the magnetic field, are used. Three boundary crossings have been selected to understand the structure of the reconnection region in detail. The transition between the boundary layer and the magnetosphere is marked by the blue bar, and between the boundary layer and the magnetosheath is marked by the red bar. The electric field spectrograms (1 s time resolution) from STAFF are displayed in extended timescale from 19:01:00 UT to 19:04:00 UT and from 19:06:00 UT to 19:09:00 UT on the magnetospheric side and from 19:15:00 UT to 19:18:00 UT on the magnetosheath side in Figure 3g. The spectrograms are used to determine the location of the separatrices (black dashed lines) on both the magnetospheric and magnetosheath sides where the wave emissions in high-frequency range (> 200 Hz) become more intense and broader [*Retinò et al.*, 2006]. C3 crossed the separatrix on the magnetospheric side twice at 19:02:35 ± 1.5 s UT and 19:07:19 ± 0.5 s UT.

The separatrix on the magnetospheric side can also be identified from a sharp change in the parallel electron differential flux (4 s time resolution) at 19:02:36 ± 2 s UT and 19:07:23 ± 2 s UT, i.e., from a magnetosheath electron population with a typical energy of several hundreds eV to a magnetospheric population of several keV (Figure 3c) [*Lindstedt et al.*, 2009]. The separatrix on the magnetosheath side was observed at 19:16:53 ± 0.5 s UT when there was a sharp decrease in the wave emissions in the high-frequency range. This separatrix can also be identified from a decrease in the electron flux antiparallel to the magnetic field at 19:16:51 ± 2 s UT. Considering the data resolution, the identifications of the separatrix from two different instrument measurements are consistent with each other. The separatrix angle ($\theta_s$), which is the angle from the current sheet to the separatrix, can be calculated by taking the ratio of the magnetic fields at the separatrix, $\theta_s \approx \tan^{-1}(B_N/B_L)$ [*Xiao et al.*, 2007].

The separatrix angle derived from the second separatrix crossing is −5° ± 1°, which is similar with the separatrix angle (−5.5° ± 1°) derived from the first crossing at 19:02:34 ± 0.5 s UT, indicating that the structure of the magnetic reconnection did not change while C3 crossed the separatrix twice. The magnetosheath side separatrix angle was 18° ± 1.5° (Figure 3j). The error bars were obtained from a propagation error analysis with data resolutions for each instrument. The separatrix angle on the magnetosheath side is much larger than that on the magnetospheric side, indicating an asymmetric magnetic reconnection geometry.

There are three ways to identify the flow boundary (gray dashed lines), the density gradients (Figure 3h) [*Vaivads et al.*, 2010; *Lindstedt et al.*, 2009], the velocity changes (Figure 3i) [*Lindstedt et al.*, 2009; *Gosling et al.*, 1990b], and the ion energy spectrum (Figure 3a) [*Lindstedt et al.*, 2009]. We used all three ways to identify

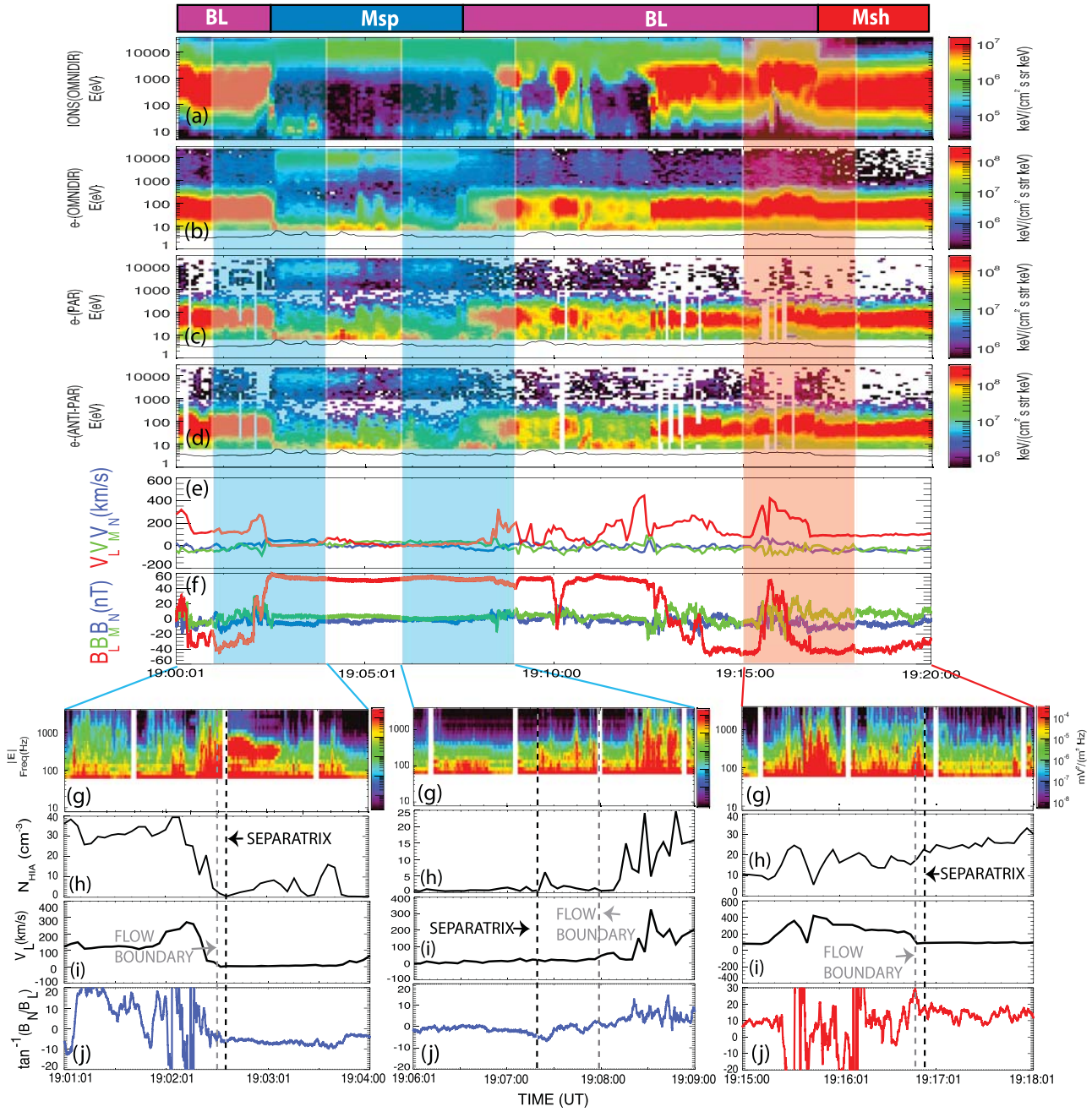


**Figure 3.** Extended timescale observations from C3. Two blue bars and a red bar show the separatrix crossings on magnetospheric and magnetosheath side. (a) Energy spectrogram of ions; (b) electron differential flux (omnidirection); (c and d) electron differential flux parallel and antiparallel to the magnetic field; (e and f) velocity and magnetic field projected in the LMN coordinate system, respectively; (g) electric field spectrogram from 19:01:00 UT to 19:04:00 UT (left), from 19:06:00 UT to 19:09:00 UT (middle), and from 19:15:00 UT to 19:18:00 UT (right); (h) plasma flow, $V_L$ component; (i) plasma density; and (j) arctangent of $B_N/B_L$.

the flow boundary on the magnetospheric side, which was observed at 19:02:31 ± 2 s UT and at 19:08:00 ± 2 s UT. However, the flow boundary on the magnetosheath side is hard to identify using the density changes because the density on the magnetosheath side of the reconnection region is already high. Therefore, *Gosling et al.* [1990b] used the velocity changes to identify the flow boundary (ion edge), and *Lindstedt et al.* [2009] identified the flow boundary using the velocity changes of $V_L$ and the ion energy spectrum on the magnetosheath side, which are the same criteria as we used, and it was observed at 19:16:47 ± 2 s UT.

The angle of flow boundary relative to the current sheet can be obtained by using the simple trigonometry (see Figure 4a). If the structure is stable and moves at a constant speed along the direction normal to the

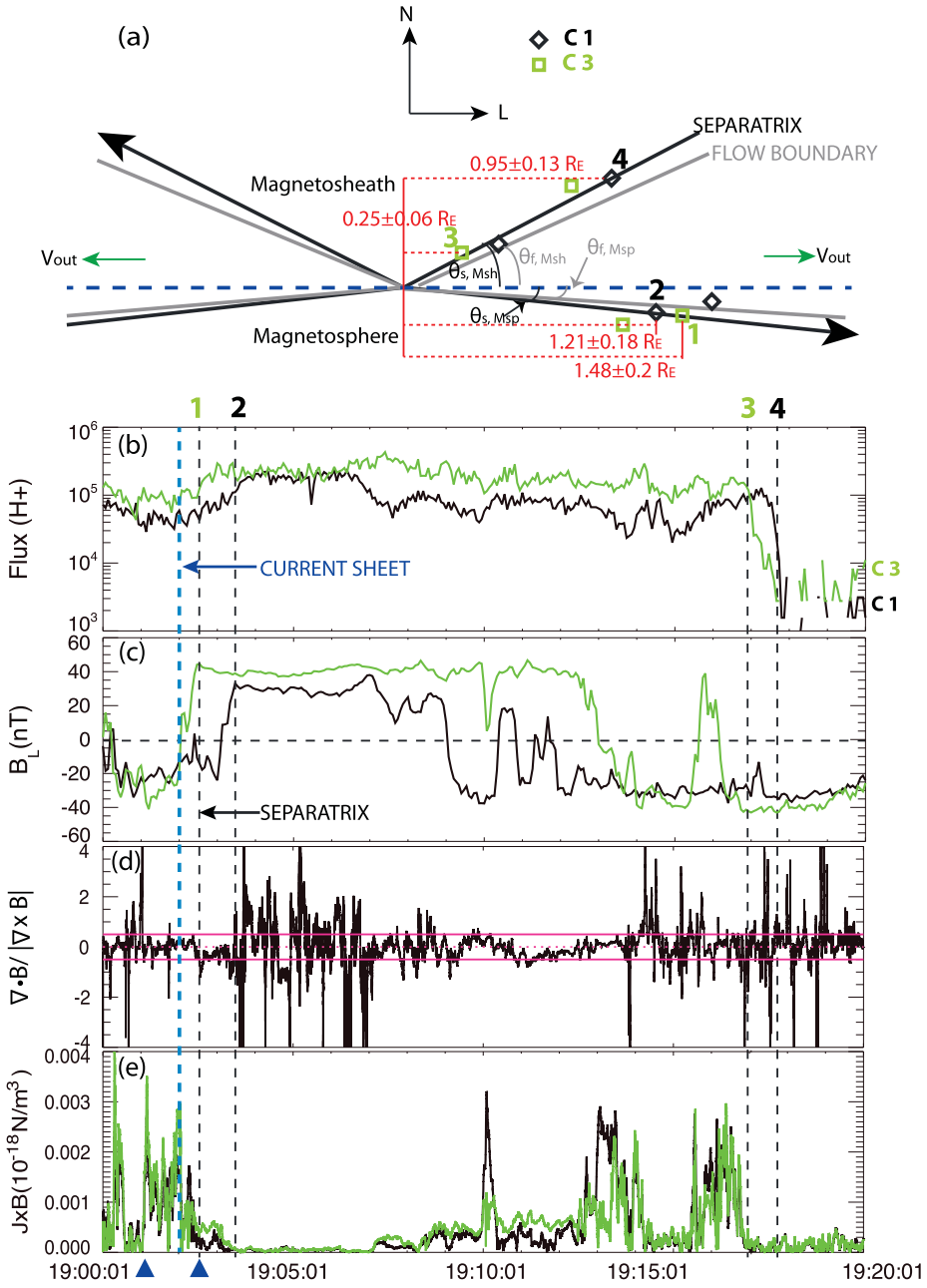


**Figure 4.** (a) A sketch of the asymmetric reconnection geometry with different separatrix angles ($\theta_s$) and the flow boundary angles ($\theta_f$), $\theta_{s,\text{magnetosheath}} = 18° \pm 1.5°$, $\theta_{s,\text{magnetosphere}} = -5.5° \pm 1°$, $\theta_{f,\text{magnetosheath}} = 15.6° \pm 1.7°$, and $\theta_{f,\text{magnetosphere}} = -4.6° \pm 0.9°$ in the boundary normal coordinates, assuming the motion of structure is stable and moves at a constant speed along the direction normal to the magnetopause. Numbers "1" and "3" ("2" and "4") mark the times when C3 (C1) cross the separatrices (e.g., 1 is the time when C3 crosses the separatrix on the magnetospheric side). The red numbers show the distances from the X line to the locations of the C1 and C3 at the separatrices. (b) Differential flux of energetic protons, (c) $B_L$ component, (d) error of current calculation, and (e) $\mathbf{J} \times \mathbf{B}$ force density observed by C1 and C3. The separatrices are marked by black dashed lines, and the current sheet crossings are marked by blue dashed lines.

magnetopause, time intervals taken from the current sheet (blue dashed line) to the flow boundary (gray solid line) and to the separatrix (black solid line) are proportional to the distances. The velocities of the structure along the normal direction, while crossing the current sheet and the separatrix on the magnetospheric side, are 28.5 ± 3.6 km/s and 26.7 ± 1.1 km/s, respectively. The normal velocities obtained from two different boundary crossings by the timing method are similar, so the assumption is reasonable. We obtain the time

intervals, $t_s = 32 \pm 1.5$ s and $t_f = 27 \pm 2$ s, to approach the separatrix and the flow boundary from the current sheet during 19:01:00 UT–19:04:00 UT, respectively, and the separatrix angle ($\theta_{s,\text{magnetosphere}} = -5.5° \pm 1°$) on the magnetospheric side, allowing the flow boundary angle ($\theta_f$) to be estimated at $\theta_f \approx \tan^{-1}(t_f/(t_s/\tan\theta_s))$. The flow boundary angle on the magnetospheric side is $-4.6 \pm 0.9°$. The flow boundary angle on the magnetosheath side can be also obtained as $15.6° \pm 1.7°$ by taking $t_s = 42 \pm 0.5$ s, $t_f = 36 \pm 2$ s, and $\theta_{s,\text{magnetosheath}} = 18° \pm 1.5°$.

The separatrix angle ($\theta_{s,\text{magnetosheath}}$) and flow boundary angle ($\theta_{f,\text{magnetosheath}}$) on the magnetosheath side are larger than those on the magnetospheric side (strongly asymmetric). Then the geometry of the asymmetric reconnection can be deduced with different separatrix and flow boundary angles and illustrated in Figure 4a. C1 crossed the separatrix on the magnetospheric (magnetosheath) side at 19:03:38 ± 0.5 s UT (19:17:48 ± 2 s UT) with separatrix angles, $-6.5° \pm 0.5°(18° \pm 1°)$. The flow boundary was observed by C1 at 19:03:34 ± 2 s UT with flow boundary angle $-5.7° \pm 0.6°$ on the magnetospheric side and at 19:17:28 ± 2 s UT with $17° \pm 1°$ on the magnetosheath side.

The joint variance analysis [*Mozer and Retinò*, 2007] has also been applied for the asymmetric magnetic reconnection. Results from the joint variance analysis are similar to those from the MVA of the magnetic field (18% differences for the magnetospheric side separatrix angles and 5% for the magnetosheath side separatrix angles). Results from both methods show that the separatrix angle on the magnetosheath side is larger than that on the magnetospheric side.

C1 (black square) and C3 (green square) configurations are also illustrated in the LMN reference frame, while they were crossing the separatrices several times on the magnetospheric and the magnetosheath sides (Figure 4a). The distances of C3 and C1 from the X line can be estimated by using the separatrix angles, velocity of the structure along the normal direction, and the time differences from the current sheet to the separatrix. For example, using the time interval, 32 s, which C3 takes from the current sheet to the separatrix on the magnetospheric side, and the velocity of the structure along the normal direction, 28.5 km/s, the distance ($h = V \times t$) from the current sheet to the separatrix is $0.14 \pm 0.02\ R_E$. And taking the tangent of the separatrix angle ($\ell = \text{h}/\tan\theta_s$), the distances ($\ell$, red numbers) from the X line to the location of the C3 and C1 on the magnetospheric side (magnetosheath side) can be obtained as $1.48 \pm 0.2\ R_E$ ($0.25 \pm 0.06\ R_E$) and $1.21 \pm 0.18\ R_E$ ($0.95 \pm 0.13\ R_E$), respectively.

The RAPID experiment on board Cluster measures 3-D energetic proton fluxes in the energy range above 30 keV (Figure 4b) and FGM measures *L* component of the magnetic field observed by C1 (black line) and C3 (green line) (Figure 4c). In the plot we have identified several separatrix crossings labeled 1 to 4 with black dashed lines (e.g., 1 marks the time when C3 crosses the separatrix on the magnetospheric side). The flux detected by C3 was higher than that detected by C1 because C3 is closer to the equator and the X line. The distances (numbers in red color) from the X line are approximately the same within the error bar when C1 and C3 crossed the separatrix on the magnetospheric side (1 and 2) so that same amount of fluxes were detected (Figure 4b); on the other hand, more energetic protons were observed by C3 than C1 when they crossed the separatrix on the magnetosheath side (3 and 4) because C1 was further away from the X line.

The current sheets are marked by blue dashed lines, the separatrices by black dashed lines. The left boundaries cover the inbound pass of the magnetopause while those on the right describe its outbound pass. The current can be calculated from the curl of the magnetic fields measured by the four spacecraft using the curlometer method. The quantity $\nabla \cdot \text{B}/|\nabla \times \text{B}|$ can be used as an estimate of the error, $\Delta J/J$ [*Robert et al.*, 1998]. Most of the values of $\nabla \cdot \text{B}/|\nabla \times \text{B}|$ (the error of current density calculation) are between ±0.5, indicating that the current calculation is reliable, in general (Figure 4d). The $\mathbf{J} \times \mathbf{B}$ force density on the magnetosheath side is approximately $0.0018\ 10^{-18}$ N/m$^3$ from 19:01:06 (marked by blue triangles) to 19:02:04 UT (blue dashed line, i.e., the current sheet), while that on the magnetospheric side is about $0.0005\ 10^{-18}$ N/m$^3$ from 19:02:04 (blue dashed line, i.e., the current sheet) to 19:02:36 UT (marked by blue triangles) for C3 (Figure 4e). The force is larger on the magnetosheath side of the reconnection region than that on the magnetospheric side.

### 2.4. Cold and Energetic Ion Behaviors

Both cold ions (5–30 eV) and energetic ions (>10 keV) were present in the magnetosphere from 19:02:20 to 19:05:00 UT (Figure 5a). The motion of the cold ions were initially perpendicular to the magnetic field (Figure 5b) and were accelerated perpendicular to the magnetic field between the separatrix and the flow boundary and beyond the flow boundary (Figures 5c–5e). The pitch angle of the magnetospheric ions

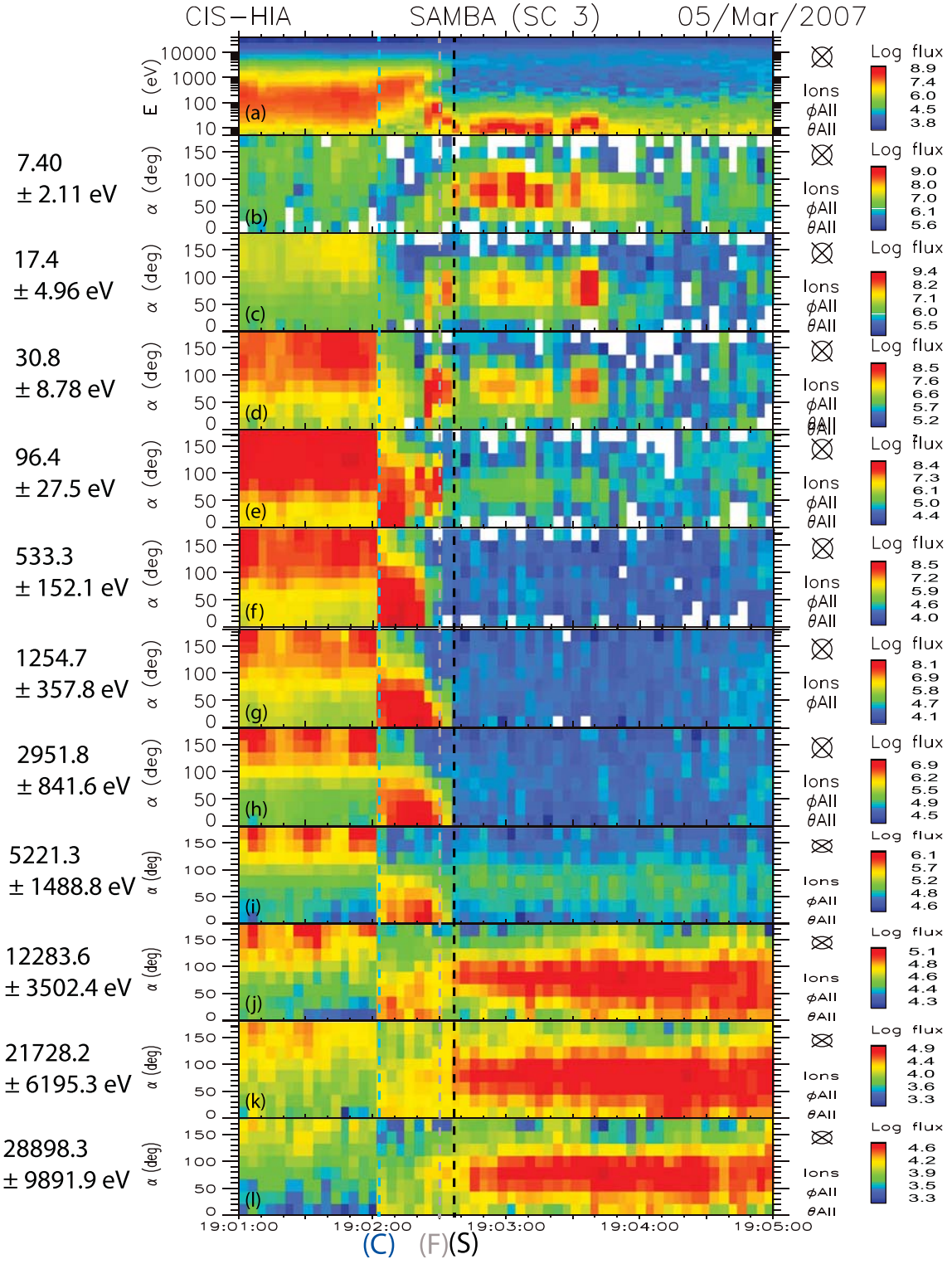


**Figure 5.** (a) Ion energy spectrum and (b–l) pitch angle distributions with different energy channels from 19:01:00 to 19:05:00 UT. Boundaries marked by vertical dashed lines are the separatrix (black dashed line, (S)), the flow boundary (gray dashed line, (F)), and the current sheet (blue dashed line, (C)).

(>10 keV) peaked at 90° in the magnetosphere. The energetic ions also moved perpendicular to the magnetic field between the separatrix and the flow boundary. Then the pitch angle of the energetic ions peaked at 0° from 19:02:04 UT to 19:02:31 UT (between the blue dashed line and the black dashed line) and 180° from 19:01:00 UT to 19:02:04 UT (inside the blue dashed line) (Figures 5j–5l). Mixture of magnetospheric and

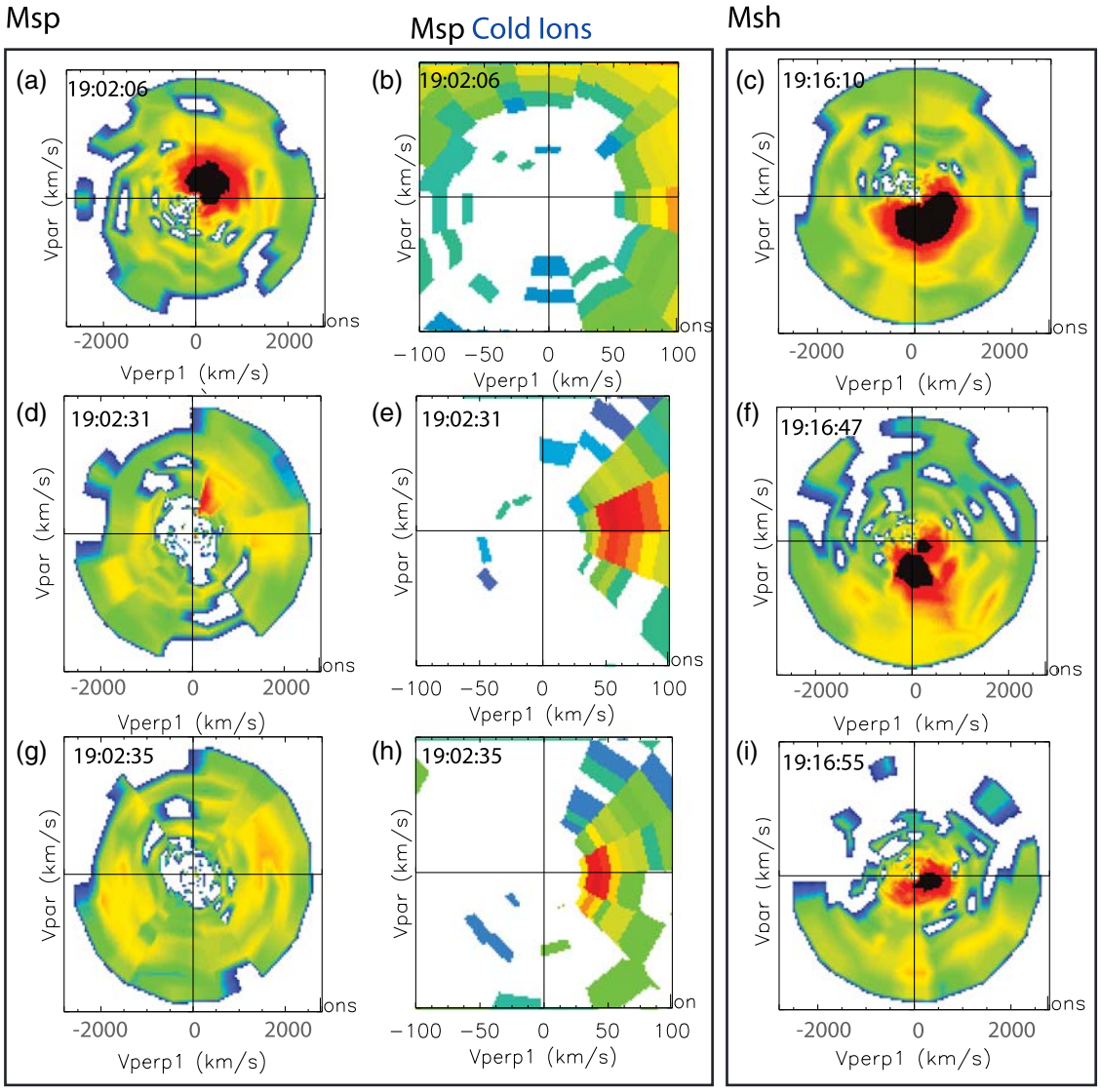


**Figure 6.** Two-dimensional cuts of the three-dimensional ion distributions obtained while C3 is (a–c) near the current sheet, (d–f) at the flow boundary, and (g–i) at the separatrix. There are three ion populations: the thermal and the energetic magnetospheric ions, the cold ions originating from the plasmasphere, and the transmitted magnetosheath ions. The cold ion behavior is different from the behaviors of the transmitted magnetosheath ions and thermal and energetic magnetospheric ions.

magnetosheath ions (Figures 5e–5i, 100 eV–10 keV) moved parallel to the magnetic field on the magnetospheric side of the reconnection region (0° pitch angle) and antiparallel to the magnetic field on the magnetosheath side (180° pitch angle ). The cold ions were not observed on the magnetosheath side of the current sheet.

The energetic ions were observed in the boundary layer during the reconnection process. The energetic ions (>10 keV) have 90° pitch angle outside of the reconnection region in the magnetosphere (Figures 5j–5l). Once they entered the reconnection region, the pitch angle changed to 0° on the magnetospheric side of the reconnection region, then to 180° on the magnetosheath side. The observed pitch angle distributions are consistent with the reconnection picture: The energetic ions flow into the reconnection region from the magnetosphere and participate the reconnection process, then they are accelerated together with other magnetosheath ions and thermal magnetospheric ions by the reconnection and observed in the outflow region.

Figure 6 shows nine examples of two-dimensional cuts through the three-dimensional distributions observed while C3 is near the current sheet (Figures 6a–6c), at the flow boundary (Figures 6d–6f), and at the

separatrix (Figures 6g–6i). The horizontal and vertical axes denote velocity components perpendicular and parallel to the magnetic field, respectively. There were two ion populations detected simultaneously at the separatrix on the magnetospheric side in Figures 6g and 6h: one was the cold dense plasmaspheric ions with energies of the order of 10 eV and the other, the hot magnetospheric ions with energy above ~10 keV. Both populations were flowing perpendicular to the magnetic field. The magnetosheath ions also moved perpendicular to the magnetic field (Figure 6i). The thermal and energetic magnetospheric ions moved parallel to the magnetic field at the flow boundary (Figure 6d), and the magnetosheath ions moved antiparallel to the magnetic field (Figure 6f), while the cold ions were accelerated with near-zero parallel velocity as shown in Figure 6e by comparing the perpendicular velocity in Figure 6h. The mixture of the magnetospheric ions and transmitted magnetosheath ions were flowing parallel and antiparallel to the magnetic field, respectively, in Figures 6a and 6c. The cold ions were not observed on the magnetosheath side of the reconnection region, i.e., inside the flow boundary (Figure 6b).

## 3. Discussion

### 3.1. Asymmetric Reconnection Geometry

In the previous section, we have shown that the flow boundary angle on the magnetospheric side is $-4.6° \pm 0.9°$ and on the magnetosheath side is $15.6° \pm 1.7°$, and the separatrix angle on the magnetospheric side is $\theta_s = -6.5° \pm 0.5°$ and $18° \pm 1°$ on the magnetosheath side. These results show a significant asymmetric reconnection geometry at the dayside magnetopause. How can we understand the asymmetric reconnection geometry at the dayside magnetopause?

In MHD simulations, the location of the X line has been predicted by using the conservation of magnetic energy flux and follows $\delta_{X2}/\delta_{X1} \approx B_2/B_1$, where $\delta_{X1,2}$ are the distances between the upstream edges of the dissipation region and the X line [*Cassak and Shay*, 2009]. For asymmetric reconnection, it has been shown by MHD simulation that the X line and stagnation point are not colocated, enabling the bulk plasma inflow to cross the X line. The X line is offset toward the side with weaker magnetic field and sub-Alfvénic flow compared to that with the stronger magnetic field and the super-Alfvénic flow since it takes more energy to bend the magnetic fields on the strong field side, and the stagnation point is offset toward whichever side has the smaller value of $\rho/B$ [*Cassak and Shay*, 2007; *Birn et al.*, 2008; *Cassak and Shay*, 2009]. If the X line moves toward the magnetosheath side, the separatrix angle on the magnetosheath side should be smaller than that on the magnetospheric side, which is opposite to the results obtained in this paper.

In this paper, we have analyzed in detail boundaries of the reconnection region and found an asymmetric structure, i.e., the separatrix and flow boundary angles and the $\mathbf{J} \times \mathbf{B}$ force density on the magnetosheath side are larger than those on the magnetospheric side. Acceleration of a higher-density plasma requires a larger $\mathbf{J} \times \mathbf{B}$ force density, which is proportional to the square root of density and magnetic field ($\mathbf{J} \times \mathbf{B} = \mathbf{F} = \mathrm{nm}\mathbf{a} = \mathrm{nm}\mathbf{V}_\mathrm{A}/t = \mathrm{nm}\mathbf{B}/(\sqrt{\mu_0 \mathrm{nm}}t) \propto \sqrt{n}\mathbf{B}$). The $\mathbf{J} \times \mathbf{B}$ force density is also proportional to the tangent of the separatrix angle ($\mathbf{J} \times \mathbf{B}$ force density $\propto \tan(\theta_s)$). This causes the separatrix angle on the magnetosheath side to be larger than that on the magnetospheric side because the density ratio (~13) of the magnetosheath to the magnetospheric side is larger than magnetic field ratio (~1.2) of two sides. The larger force on the magnetosheath side can shift the X line toward the magnetospheric side which is consistent with the results from *Mozer et al.* [2008].

### 3.2. Can Cold Ions Affect the Reconnection Dynamics?

The cold ions (5–30 eV) with near-zero parallel velocity were observed at the separatrix (Figure 7a). As can be seen from Figure 7b, once the cold ions were energized, three cold ion populations (probably $H^+$, $He^+$, and $O^+$) appeared in the energy spectrum because they have different masses and were accelerated to the same velocity (~100 km/s). Helium ($He^+$) and oxygen ions ($O^+$) were energized 4 and 16 times higher than that of the proton ($H^+$). *Borovsky and Steinberg* [2006] hypothesized that high-density plasma could reduce the local Alfvén speeds, and *Borovsky and Denton* [2006] noticed reductions in the amount of solar wind/magnetosphere coupling during geomagnetic storms when very high density plasma from the plasmasphere was convected into the dayside reconnection site. In a simulation study, *Borovsky et al.* [2008] showed a spatially localized plume of plasma can reduce the reconnection rate by about a factor of 2. However, the accelerated cold ions motion we have observed were perpendicular to the magnetic field. If they were accelerated by the reconnection process like the thermal and energetic magnetospheric ions, they would have velocity parallel to the magnetic field. In addition, the cold ions should be observed in the outflow region with other accelerated particles if they flow into the diffusion region and participate the

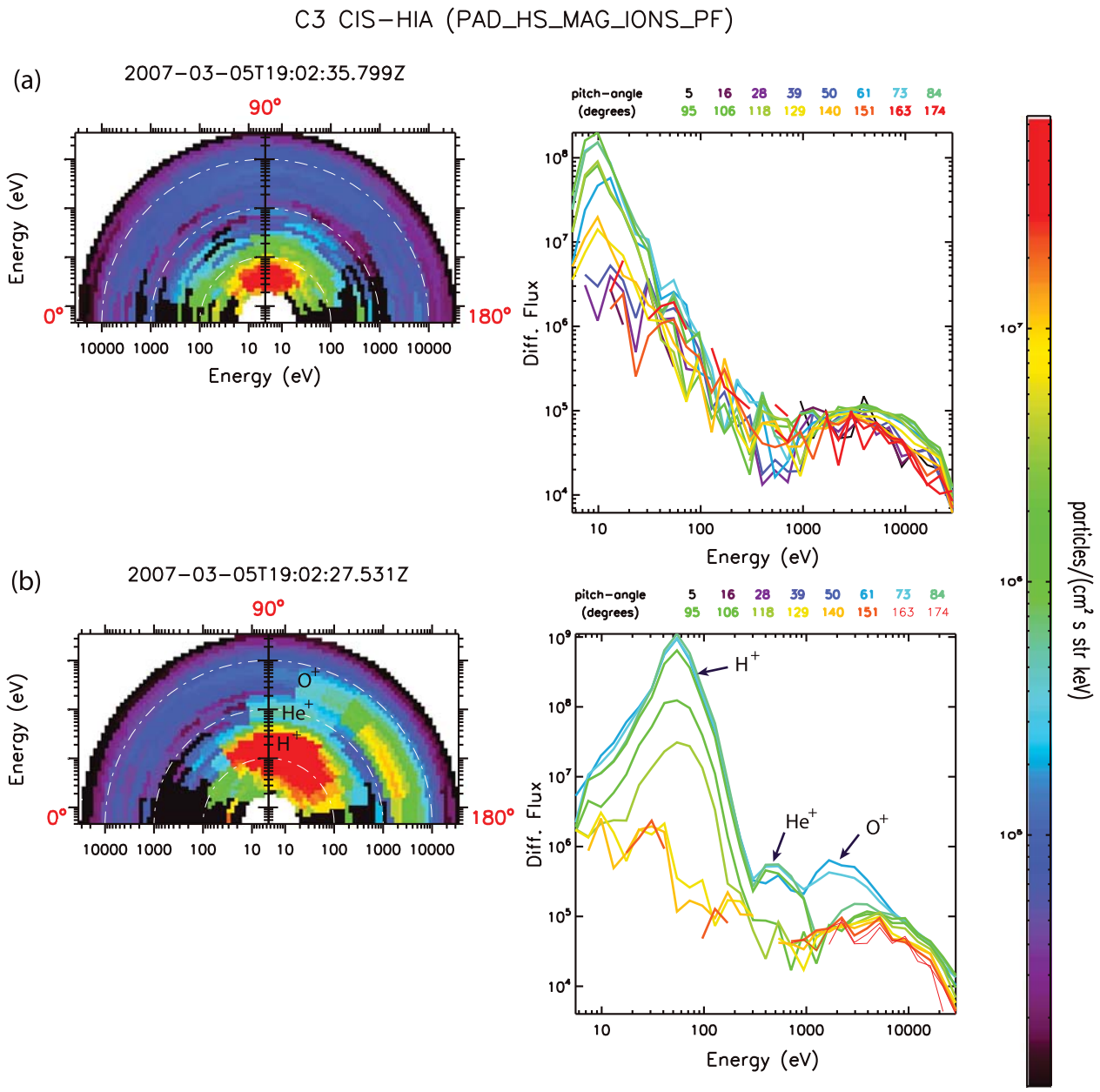


**Figure 7.** The energy spectra of cold ions with different pitch angles during the magnetic reconnection (a) at the separatrix and (b) inside the flow boundary. The cold dense plasmaspheric ions with near-zero parallel velocity were observed at the separatrix (Figure 7a) and were accelerated perpendicular to the magnetic field inside the flow boundary (Figure 7b). Three cold ion populations (probably $H^+$, $He^+$, and $O^+$) appear in the energy spectrum because they have different masses and were accelerated to the same velocity (~100 km/s).

reconnection process. However, the cold ions were observed only near the separatrix and the flow boundary on the magnetospheric side. Therefore, the cold ions did not participate in the reconnection process.

The schematic drawings of the motion of the thermal and energetic magnetospheric ions (red arrows), cold ions (blue arrows), and the magnetosheath ions (dark green arrows) in the dHT frame (where the convection electric field vanishes) are illustrated in Figure 8. Thermal and energetic magnetospheric ions and the magnetosheath ions were accelerated with large parallel velocities by the reconnection process and away from the X line as shown in Figure 8a. The cold plasmaspheric ion flow into the reconnection outflow region by the $\mathbf{E} \times \mathbf{B}$ drift rather than into the diffusion region near the subsolar magnetopause (Figure 8b). Thus, the cold ions are picked up by newly reconnected field line at high latitude and accelerated by the convection electric field perpendicular to the magnetic field, which is similar to the pickup ion process in the solar wind.

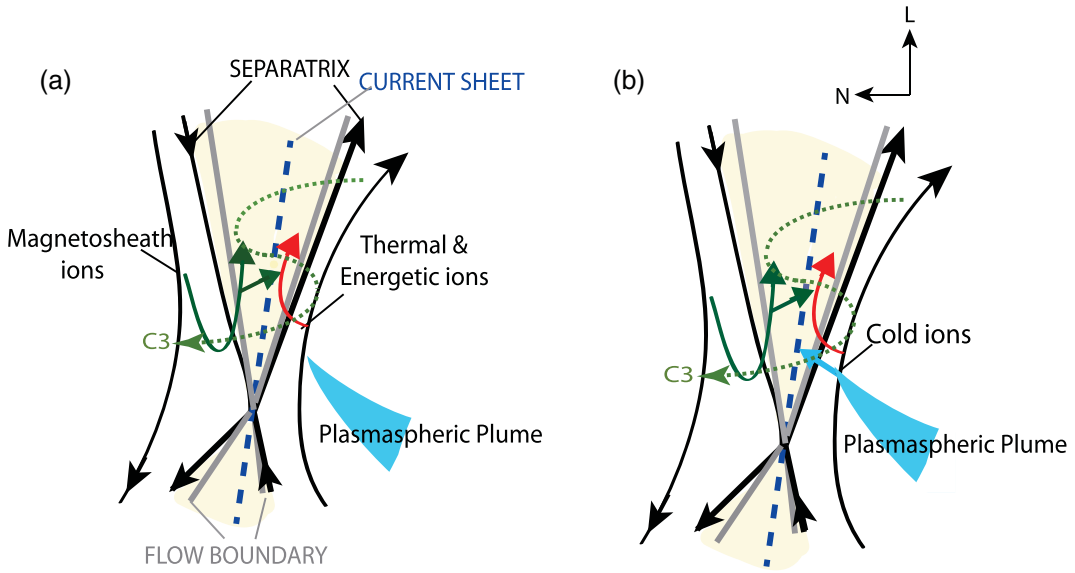


**Figure 8.** Reconnection configuration with qualitative sketch of the motion of cold (blue arrow), thermal and energetic magnetospheric ions (red arrow), and magnetosheath ions (dark green arrows) in the dHT frame. (a) The transmitted magnetosheath ions and thermal and energetic ions are accelerated by the reconnection process. The source of the cold ions in reconnection can be plumes detached from the plasmasphere. The cold ions flow into the reconnection outflow region by the $\mathbf{E} \times \mathbf{B}$ drift. (b) They are picked up by newly reconnected field line and accelerated by the convection electric field perpendicular to the magnetic field. The green dotted line shows the spacecraft (C3) trajectory. The black lines, which are connected to the X line, denote the separatrices; the gray lines correspond to the flow boundaries; the blue dashed line marks the current sheet crossings; and the yellow area shows the reconnection region.

Behavior of the cold ions in our observations agrees with the test particle simulation results from *Drake et al.* [2009]. *Drake et al.* [2009] showed that heavy ions crossing the separatrix into the exhaust behave like pickup ions, which perform a cycloidal motion in the plane perpendicular to the guide field and gain perpendicular energy. Our observations show that the cold ions also behave like pickup ions, which were carried into the reconnection region by the reconnected field line and gain perpendicular energy. *Gosling et al.* [1990a] also observed a cold ion beam whose speed was always less than the transmitted magnetosheath ions although both populations shared the same $\mathbf{E} \times \mathbf{B}$ drift. They suggested that the cold beams are accelerated simply by being tied to the field lines. Our observations are consistent with those of *Gosling et al.* [1990a].

## 4. Summary and Conclusions

We have presented a study of an asymmetric magnetic reconnection event on 5 March 2007 at the dayside magnetopause. Separatrices and flow boundaries on both the magnetospheric and magnetosheath sides are identified by sharp changes in the electromagnetic wave spectrogram, particle differential flux, plasma flow, magnetic field, and density gradients. The cold plasmaspheric ions (5–30 eV) are observed on the magnetospheric side of the current sheet, and the energetic protons, helium, (> 30 keV), and oxygen ions (> 84 keV) are also observed in the reconnection region. The significant observations can be summarized as follows:

1. The separatrix and flow boundary angles on the magnetosheath side are larger than those on the magnetospheric side. This may be caused by the stronger asymmetry in the plasma density than that in the magnetic field.
2. The asymmetric geometry of the magnetic reconnection is obtained by different separatrix angles on both sides of the current sheet.
3. The cold dense plasmaspheric ions are picked up by recently reconnected field lines at higher latitude rather than in the diffusion region near the subsolar magnetopause. These cold ions are accelerated by the electric field perpendicular to the magnetic field and carried by the reconnection convection flow which is similar to the pickup ion process.

4. Three cold ion populations (probably $H^+$, $He^+$, and $O^+$) appear in the energy spectrum because they have different masses and are accelerated to the same velocity.
5. The observed pitch angle distributions for the energetic ions (> 10 keV) in the boundary layer are consistent with the reconnection picture.

**Acknowledgments**
We thank all of those who have made the Cluster mission for the successful spacecraft operation and for the high-quality data. This work was carried out while S.H. Lee held a NASA Earth and Space Science Fellowship. K.H.G. was financially supported through grants 50OC1102 and 50OC1001 by the German Bundesministerium für Wirtschaft und Technologie and the Deutsches Zentrum für Luft- und Raumfahrt.

Masaki Fujimoto thanks the reviewers for their assistance in evaluating this paper.

## References

André, M., A. Vaivads, Y. V. Khotyaintsev, T. Laitinen, H. Nilsson, G. Stenberg, A. Fazakerley, and J. G. Trotignon (2010), Magnetic reconnection and cold plasma at the magnetopause, *Geophys. Res. Lett.*, *37*, L22108, doi:10.1029/2010GL044611.

Balogh, A., et al. (1997), The Cluster magnetic field investigation, *Space Sci. Rev.*, *79*, 65–91.

Birn, J., J. E. Borovsky, and M. Hesse (2008), Properties of asymmetric magnetic reconnection, *Phys. Plasmas*, *15*, 032,101, doi:10.1063/1.2888491.

Borovsky, J. E., and M. H. Denton (2006), Effect of plasmaspheric drainage plumes on solar-wind/magnetosphere coupling, *Geophys. Res. Lett.*, *33*, L20101, doi:10.1029/2006GL026519.

Borovsky, J. E., and M. Hesse (2007), The reconnection of magnetic fields between plasmas with different densities: Scaling relations, *Phys. Plasmas*, *14*, 102,309, doi:10.1063/1.2772619.

Borovsky, J. E., and J. T. Steinberg (2006), The "calm before the storm" in CIR/magnetosphere interactions: Occurrence statistics, solar wind statistics, and magnetospheric preconditioning, *J. Geophys. Res.*, *111*, A07S10, doi:10.1029/2005JA011397.

Borovsky, J. E., M. Hesse, J. Birn, and M. M. Kuznetsova (2008), What determines the reconnection rate at the dayside magnetosphere?, *J. Geophys. Res.*, *113*, A07210, doi:10.1029/2007JA012645.

Cassak, P. A., and M. A. Shay (2007), Scaling of asymmetric magnetic reconnection: General theory and collisional simulations, *Phys. Plasmas*, *14*, 102,114, doi:10.1063/1.2795630.

Cassak, P. A., and M. A. Shay (2008), Scaling of asymmetric Hall magnetic reconnection, *Geophys. Res. Lett.*, *35*, L19102, doi:10.1029/2008GL035268.

Cassak, P. A., and M. A. Shay (2009), Structure of the dissipation region in fluid simulations of asymmetric magnetic reconnection, *Phys. Plasmas*, *16*, doi:10.1063/1.3086867.

Cattell, C., et al. (2005), Cluster observations of electron holes in association with magnetotail reconnection and comparison to simulations, *J. Geophys. Res.*, *110*, A01211, doi:10.1029/2004JA010519.

Cornilleau-Wehrlin, N., et al. (2003), First results obtained by the Cluster STAFF experiment, *Ann. Geophys.*, *21*, 437–456, doi:10.5194/angeo-21-437-2003.

Cowley, S. W. H. (1982), The causes of convection in the Earth's magnetosphere: A review of developments during the IMS, *Rev. Geophys.*, *20*, 531–565.

Deng, X. H., and H. Matsumoto (2001), Rapid magnetic reconnection in the Earth's magnetosphere mediated by whistler waves, *Nature*, *410*, 557–560, doi:10.1038/410557A0.

Drake, J. F., M. Swisdak, T. D. Phan, P. A. Cassak, M. A. Shay, S. T. Lepri, R. P. Lin, E. Quataert, and T. H. Zurbuchen (2009), Ion heating resulting from pickup in magnetic reconnection exhausts, *J. Geophys. Res.*, *114*, A05111, doi:10.1029/2008JA013701.

Dungey, J. W. (1961), Interplanetary magnetic field and the auroral zones, *Phys. Rev. Lett.*, *6*, 47–48.

Escoubet, C. P., R. Schmidt, and M. L. Goldstein (1997), Cluster—Science and mission overview, *Space Sci. Rev.*, *79*, 11–32.

Fairfield, D. H. (1971), Average and unusual locations of the Earth's magnetopause and bow shock, *J. Geophys. Res.*, *76*, 6700–6716.

Gosling, J. T., M. F. Thomsen, S. J. Bame, R. C. Elphic, and C. T. Russell (1990a), Cold ion beams in the low latitude boundary layer during accelerated flow events, *Geophys. Res. Lett.*, *17*, 2245–2248, doi:10.1029/GL017i012p02245.

Gosling, J. T., M. F. Thomsen, S. J. Bame, T. G. Onsager, and C. T. Russell (1990b), The electron edge of the low latitude boundary layer during accelerated flow events, *Geophys. Res. Lett.*, *17*, 1833–1836.

Lin, R. P., et al. (2003), RHESSI observations of particle acceleration and energy release in an intense solar gamma-ray line flare, *Astrophys. J. Lett.*, *595*, L69–L76, doi:10.1086/378932.

Lindstedt, T., Y. V. Khotyaintsev, A. Vaivads, M. André, R. C. Fear, B. Lavraud, S. Haaland, and C. J. Owen (2009), Separatrix regions of magnetic reconnection at the magnetopause, *Ann. Geophys.*, *27*, 4039–4056, doi:10.5194/angeo-27-4039-2009.

Matsumoto, H., X. H. Deng, H. Kojima, and R. R. Anderson (2003), Observation of Electrostatic Solitary Waves associated with reconnection on the dayside magnetopause boundary, *Geophys. Res. Lett.*, *30*(6), 1326, doi:10.1029/2002GL016319.

Mozer, F. S., and P. L. Pritchett (2009), Regions associated with electron physics in asymmetric magnetic field reconnection, *Geophys. Res. Lett.*, *36*, L07102, doi:10.1029/2009GL037463.

Mozer, F. S., S. Bale, and T. D. Phan (2002), Evidence of diffusion regions at a subsolar magnetopause crossing, *Phys. Rev. Lett.*, *89*, 015,002, doi:10.1103/PhysRevLett.89.015002.

Mozer, F. S., P. L. Pritchett, J. Bonnell, D. Sundkvist, and M. T. Chang (2008), Observations and simulations of asymmetric magnetic field reconnection, *J. Geophys. Res.*, *113*, A00C03, doi:10.1029/2008JA013535.

Mozer, F. S., and A. Retinò (2007), Quantitative estimates of magnetic field reconnection properties from electric and magnetic field measurements, *J. Geophys. Res.*, *112*, A10206, doi:10.1029/2007JA012406.

Øieroset, M., T. D. Phan, M. Fujimoto, R. P. Lin, and R. P. Lepping (2001), In situ detection of collisionless reconnection in the Earth's magnetotail, *Nature*, *412*, 414–417.

Øieroset, M., R. P. Lin, T. D. Phan, D. E. Larson, and S. D. Bale (2002), Evidence for electron acceleration up to 300 keV in the magnetic reconnection diffusion region of Earth's magnetotail, *Phys. Rev. Lett.*, *89*, 195,001, doi:10.1103/PhysRevLett.89.195001.

Paschmann, G., I. Papamastorakis, N. Sckopke, G. Haerendel, B. U. Oe. Sonnerup, S. J. Bame, J. R. Asbridge, J. T. Gosling, C. T. Russel, and R. C. Elphic (1979), Plasma acceleration at the Earth's magnetopause: Evidence for reconnection, *Nature*, *282*, 243–246.

Pritchett, P. L., and F. S. Mozer (2009), Asymmetric magnetic reconnection in the presence of a guide field, *J. Geophys. Res.*, *114*, A11210, doi:10.1029/2009JA014343.

Rème, H., et al. (2001), First multispacecraft ion measurements in and near the Earth's magnetosphere with the identical Cluster ion spectrometry (CIS) experiment, *Ann. Geophys.*, *19*, 1303–1354.

Retinò, A., et al. (2006), Structure of the separatrix region close to a magnetic reconnection X-line: Cluster observations, *Geophys. Res. Lett.*, *33*, L06101, doi:10.1029/2005GL024650.

Robert, P., M. W. Dunlop, A. Roux, and G. Chanteur (1998), Accuracy of current density estimation, in *Analysis Methods for Multi Spacecraft Data*, edited by G. Paschmann and P. W. Daly, pp. 395–418, ESA, Bern, Switzerland.

Sonnerup, B. U. Ö., G. Paschmann, I. Papamastorkis, N. Sckopke, G. Haerendel, S. J. Bame, J. R. Asbridge, J. T. Gosling, and C. T. Russell (1981), Evidence for magnetic field reconnection at the Earth's magnetopause, *J. Geophys. Res.*, *86*, 10,049–10,067.

Sonnerup, B. U. Ö., I. Papamastorakis, G. Paschmann, and H. Lühr (1987), Magnetopause properties from AMPTE/IRM observations of the convection electric field: Method development, *J. Geophys. Res.*, *92*, 12,137–12,159.

Speiser, T. W., D. J. Williams, and H. A. Garcia (1981), Magnetospherically trapped ions as a source of magnetosheath energetic ions, *J. Geophys. Res.*, *86*, 723–732.

Su, Y.-J., J. E. Borovsky, M. F. Thomsen, R. C. Elphic, and D. J. McComas (2000), Plasmaspheric material at the reconnecting magnetopause, *J. Geophys. Res.*, *105*, 7591–7600, doi:10.1029/1999JA000266.

Vaivads, A., A. Retinò, Y. V. Khotyaintsev, and M. André (2010), The Alfvén edge in asymmetric reconnection, *Ann. Geophys.*, *28*, 1327–1331, doi:10.5194/angeo-28-1327-2010.

Wilken, B., et al. (2001), First results from the RAPID imaging energetic particle spectrometer on board Cluster, *Ann. Geophys.*, *19*, 1355–1366.

Xiao, C. J., et al. (2007), A Cluster measurement of fast magnetic reconnection in the magnetotail, *Geophys. Res. Lett.*, *34*, L01101, doi:10.1029/2006GL028006.

Zhang, H., Q.-G. Zong, T. A. Fritz, S. Y. Fu, S. Schaefer, K. H. Glassmeier, P. W. Daly, H. Rème, and A. Balogh (2008), Cluster observations of collisionless Hall reconnection at high-latitude magnetopause, *J. Geophys. Res.*, *113*, A03204, doi:10.1029/2007JA012769.

Zong, Q.-G., and B. Wilken (1998), Layered structure of energetic oxygen ions in the magnetosheath, *Geophys. Res. Lett.*, *25*, 4121–4124.

Zong, Q.-G., and B. Wilken (1999), Bursty energetic oxygen events in dayside magnetosheath: Geotail observation, *Geophys. Res. Lett.*, *26*, 3349–3352.

Zong, Q.-G., B. Wilken, S.-Y. Fu, T. A. Fritz, Z.-Y. Pu, N. Hasebe, and D. J. Williams (2001), Ring current oxygen ions in the magnetosheath caused by magnetic storm, *J. Geophys. Res.*, *106*, 25,541–25,556.